XXIV Biennial Symposium on Measuring Techniques in Turbomachinery
Prague, Czech Republic, 29 - 31 August 2018
Paper No MTT2418B32

# DEVELOPMENTS IN HIGH FREQUENCY DIRECTIONAL PROBES FOR HIGH TEMPERATURE APPLICATIONS

**L. Bhatnagar, J. Braun, V. Andreoli, D. Gonzalez Cuadrado, Z. Liu**
Purdue University, 47906 West Lafayette, USA

**G. Paniagua**
Purdue University & Petal Solutions LLC, 47906 West Lafayette, USA

**Keywords:** high frequency pressure probe, five-hole pressure probe, high temperature

## ABSTRACT

Aerodynamic probes disrupt the flow that attempts to measure, while suffering serious temperature limitations associated to the melting temperature of the materials used for the sensors. This manuscript presents the design methodology for a novel cooled five-hole pressure probe, miniaturized to enable high fidelity in a frequency band 0-100 kHz in high temperature environments. In a first step, the probe dimensions are selected to minimize the interference with the flow field. Three dimensional Reynolds Averaged Navier-Stokes simulations were used to characterized the aerodynamic performance, while the shape of the stem was optimized to abate the unsteady vortex shedding, using a geometry inspired from seal whiskers. Furthermore, a numerical approach is outlined to cool the probe in a high temperature and high-speed environment. Finally, we discuss the preliminary testing of the probe in the Purdue Experimental Turbine Aerothermal Lab.

## NOMENCLATURE

| | |
|---|---|
| h | height [m] |
| M | Mach number [-] |
| P | Pressure [bar] |
| $P_{Total}$ | Total Pressure [bar] |
| T | Temperature [K] |
| V | Velocity [m/s] |
| $\tau_{wall}$ | Wall Shear Stress |
| t | time |

## ABBREVIATIONS

| | |
|---|---|
| URANS | Unsteady Reynolds Averaged Navier Stokes |
| CHT | Conjugate Heat Transfer |
| CFD | Computational Fluid Dynamics |
| CFL | Courant–Friedrichs–Lewy |
| FEA | Finite Element Analysis |
| PETAL | Purdue Experimental Turbine AeroThermal Laboratory |
| CPU | Central Processing Unit |

## INTRODUCTION

Aero-engine applications operate typically in high pressure and high temperature, with very limited optical access. Therefore, multi-hole pressure probes are ubiquitous in high-pressure turbomachinery applications. Ainsworth et al. [1] and Sieverding et al. [2] presented design reviews and characteristics of multi-hole pressure probes. According to the head shape [3], a multi-hole pressure probe can be categorized into cobra, conical, pyramidal, or hemispherical. Arguelles Diaz et al. [4] tested different head geometries, namely cobra, cylindrical, and trapezoidal, to characterize the geometrical effect on the flow measurements. Their investigation demonstrated that the cobra probe evidenced the largest angular range while the cylindrical probe retrieved the lowest measurement uncertainty. Delhaye et al. [5] numerically evaluated the unsteady performance of a pyramidal probe with flush-mounted sensors and results indicated that the separation bubbles had little effect on lateral readings. Liu and Paniagua [6] designed a cylindrical five-hole probe with subsurface-mounted sensors, their numerical investigation showed a distinct vortex shedding in all the pressure readings, with a base pressure tapping insensitivity to yaw angle variations. Such a five hole-cavity-sensor arrangement protects the sensors from being damaged in harsh environments and while providing better spatial resolution than flush-mounted sensors. However, in such configuration the hole-cavity induces a resonance frequency [7]. Bergh and Tijdeman [8] developed and validated an analytical model to estimate the frequency response of different tube-cavity configurations with various tube length and tube diameter.

Five-hole probes experience vortex shedding unsteadiness due to the intrusion of the probe within the flow field, as shown in Fig. 1 [6]. Biomimicry was used to explore strategies conducting towards the suppression of the vortex induced vibration. Hanke et al. [9] demonstrated using computational tools that whisker-like vibrissa reduced the lift forces by 90% compared to the cylinder-like model. Hans et al. [10] proved that undulations on both the major and minor axis of the stem are essential to attenuate the lift force and suppress the vortex shedding. The experiments of Kottapalli et al. [11] showed that the whisker-inspired flow sensors reduced the amplitude of the

vortex shedding 50 times. Additionally, whisker-like sensors displayed high sensitivity to the underwater environments thanks to its low self-induced vibrating noise [12]. Beem et al. [13] discovered that whisker-inspired flow sensors are better than cylindrical sensors to detect wake-induced vibrations because of reduced interference of the vortex shedding in their underwater tests. Such unique detection mechanism is also used by seals: their wavy whiskers enable to capture preys with heads tarts of 30s due to reduction of excitation force by uncoupling the vortex shedding [14]. Regarding heat transfer, a numerical investigation of whisker-like pin fins augmented heat transfer by 20% compared to the cylindrical pin fins at a Reynolds number of $10^4$ [15].

This paper proposes a novel design methodology of a cooled miniature five-hole directional pressure probe able to measure at frequencies up to 100 kHz in high speed and high temperature environments, for gas turbine applications. The dimensions were selected to minimize the interference with the flow field by analyzing whisker like designs, the aerodynamic performance was characterized through three-dimensional unsteady Reynolds Averaged Navier-Stokes (URANS) simulations. Secondly, a numerical approach is outlined to be able to cool the probe for high temperature conditions. Finally, experiments in the PETAL test facilities were carried to characterize heating as well as vortex shedding.

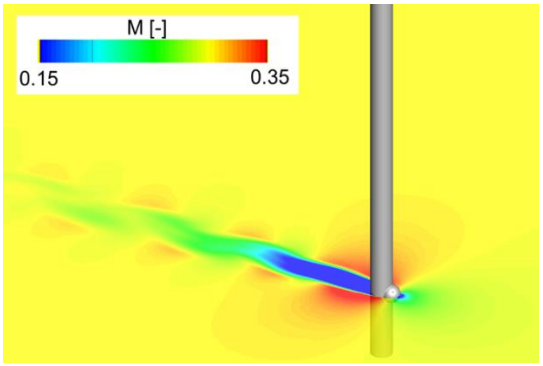


*Figure 1: Instantaneous vortex shedding down-stream of a cylindrical directional probe [6]*

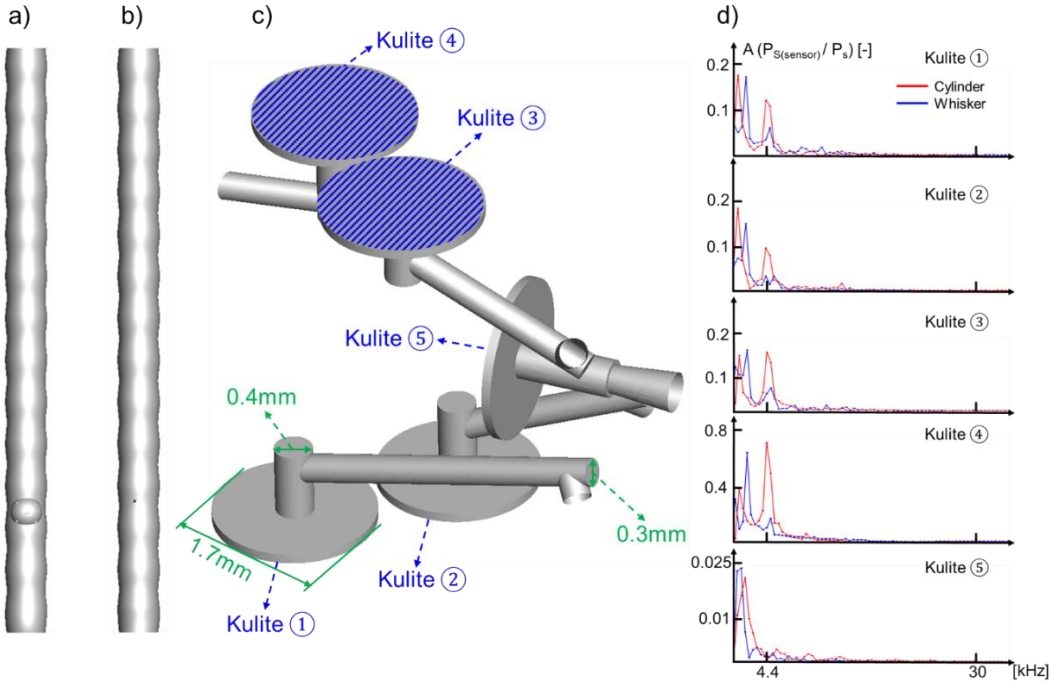


*Figure 2: a) Probe head. b) Detail of the back of the probe. c) Detail of the Kulite locations. d) Fast Fourier Transform of the five pressure sensors*

## NOVEL FIVE-HOLE PROBE WITH THE WHISKER-INSPIRED DESIGN

Figure 2a depicts the frontal view of the five-hole directional probe. Five miniature Kulite sensors are embedded inside of a 3.7 mm diameter Inconel probe. Additionally, the five recessed sensors located in the stem provide an improved performance in a wider range of Mach number, from low subsonic to transonic. The shape of the stem is inspired by the harbor seal whiskers. Figure 2b displays the location of the base pressure tapping and Fig. 2c exhibits the internal line-cavity configuration that connect the Kulites to the flow field. The internal line-cavity configurations have a diameter from 0.3 to 0.4 mm. Figure 2d shows the frequency spectrum of each recessed sensor. The simulations were carried out with three dimensional URANS simulations and solved with a second order scheme. The numerical mesh contained 7 million cells and the time-step for the

simulations was 1 μs with a total computational time of 432 hrs on 20 CPU's. The vortex shedding frequency was identified around 4.4±0.5 kHz, close to the theoretical prediction based on Strouhal-Reynolds correlations [16] and a cylindrical stem design was compared to the whisker design. In all recessed sensors, the amplitudes of the vortex shedding were reduced, up to 76% in the base tapping.

## COOLING STRATEGY

### Computational domain for the conjugate heat transfer simulations

The targeted freestream temperature is 1900K, however 548K is the maximum inner surface temperature that can be sustained by the Kulite sensors. The two-dimensional model of the probe cross-section was analyzed to determine the heat load that the cooling system needs to bear. The probe is cooled using a cooling jacket covering the probe body, which was designed using 2-dimensional strategies to first reduce computational cost and secondly to perform multiple studies varying all parameters. The first assumption is that the probe was perfectly cylindrical instead of the whisker inspired design, as shown in Figure 3a. The major axis of the elliptical cross section of the whisker probe is taken as the diameter of the simplified geometry. The effect of the central dome, shown in red in Figure 3a, and the wire passage, was neglected to create a simplified two-dimensional axisymmetric geometry with 2 pressure sensors holes as shown in Figure 3b.

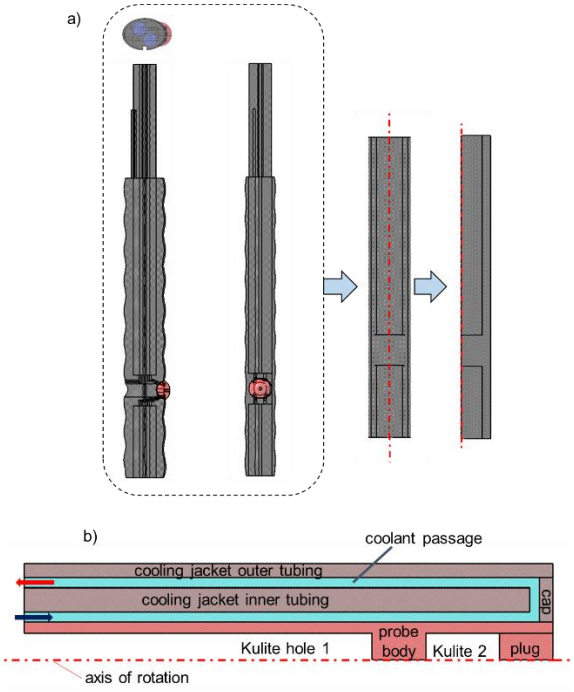


*Figure 3: a) Simplification of geometry from 3D to a 2D axisymmetric geometry. b) 2D axisymmetric geometry of the probe and cooling jacket.*

The geometry consists of a coolant passage with the coolant entering right next to the probe, where the gap between the probe body (red) and the jacket inner tubing (grey) forms the actual coolant passage. The coolant passage turns near the end of the probe body to cool the outer surface of the probe. The walls of the jacket are made from Inconel just as the probe.

Based on a Nusselt number relation [17] for flows across a cylinder and flow conditions in conventional jet engines, an estimate of the heat transfer coefficient from the flow to the probe was obtained. The Reynolds number was around $3.3X10^5$ and by applying a correction to the Nusselt number for this Reynolds number [18], an estimate of the coefficient of heat transfer as 3526.8 $W/mK$ was found.

The boundary conditions of the numerical simulations are shown on a baseline case in Figure 4a. A velocity inlet was applied and a static pressure was applied at the outlet. The outer walls had an imposed convection with a freestream temperature of 1900K and a heat transfer coefficient of 3526.8W/mK. The wall thickness of the jacket is 1 mm, based on the yield shear stress of Inconel at elevated temperature with a safety factor of 2. The coolant used is distilled water. The channel width is 3 mm and is based on an initial estimate to have a maximum coolant temperature below its boiling point with an injection of coolant flow at 10 m/s. The mesh was generated using Ansys workbench unstructured mesh generator and quadrilateral meshes were generated by varying the maximum face size to obtain different meshes.

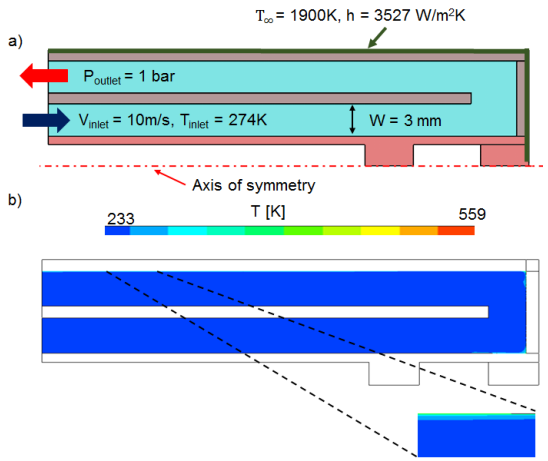


*Figure 4: a) Geometry and boundary conditions. b) Temperature Contour of the coolant channel with a zoom in on the maximum temperature area.*

The solver was Fluent and was a pressure based solver adapted for conjugate heat transfer by balancing the heat equation at the interface of the solid and fluid regions. The under relaxation factor for the pressure field was 0.3 resulting in a CFL number of 2.4. The convergence criteria were a mass flow balance at the inlet and outlet, stable value of the wall shear stress & total surface heat

transfer at each of the fluid solid interfaces and a drop to $10^{-6}$ for each residual value.

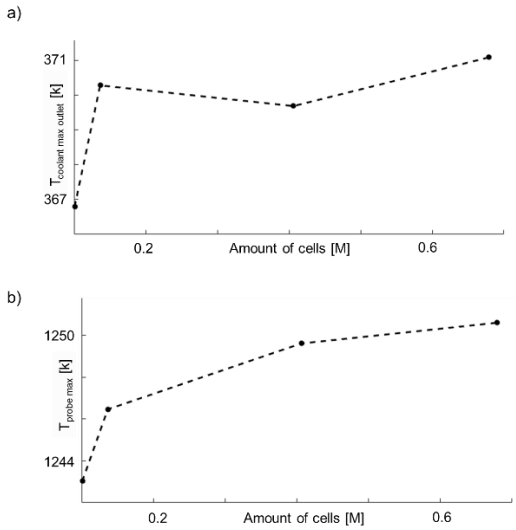


*Figure 5: a) Grid sensitivity to maximum. coolant temperature. b) maximum temperature in the system.*

A mesh sensitivity study was carried out to ensure grid independence. The maximum temperature of the coolant (Figure 5a) and the maximum temperature in the entire probe (Figure 5b) were monitored. From a medium to fine mesh, the maximum temperature of the coolant increased by only 1.4K. It is observed that the average temperature of the coolant only increased from 274 K at the inlet to 278.4K at the outlet, owing to a limited amount of heat transfer. The maximum temperature is retrieved near the outlet channel of the coolant, as shown in Figure 4b. The second hottest point was located near the first channel bend. Based on the results in Figure 5, the chosen mesh had a maximum face size of $2.5X10^{-5}$m with a total mesh count of 0.4 million cells and a y+ of 0.3.

## Parametric analysis

A parametric study is performed on geometrical features as well as on coolant inlet conditions.

Figure 6a shows the outlet channel height that was varied as the first parameter and its effect on the maximum coolant temperature and the inlet total pressure requirement is shown in Figure 6b. A drop in maximum coolant temperature at the outlet channel is observed as the channel passage is decreased. This is due to a flow velocity increase when the channel height is decreased, to maintain the same inlet mass flow and hence leading to better heat transfer. However, as evident by Figure 6b, this decrease in the channel passage height also increases the pressure requirement at the inlet due to increased pressure losses in the channel. Hence, an optimal operating condition between temperature decrease and increased pressure requirement needs to be set.

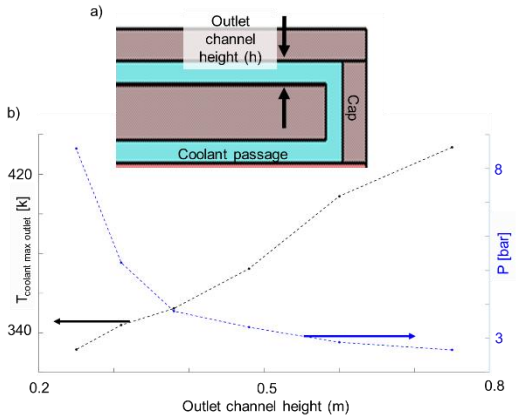


*Figure 6: a) Schematic showing the outlet channel height. b)Variation of maximum coolant temperature at the outlet and the inlet total pressure required to maintain constant mass flow of coolant with changing outlet channel height.*

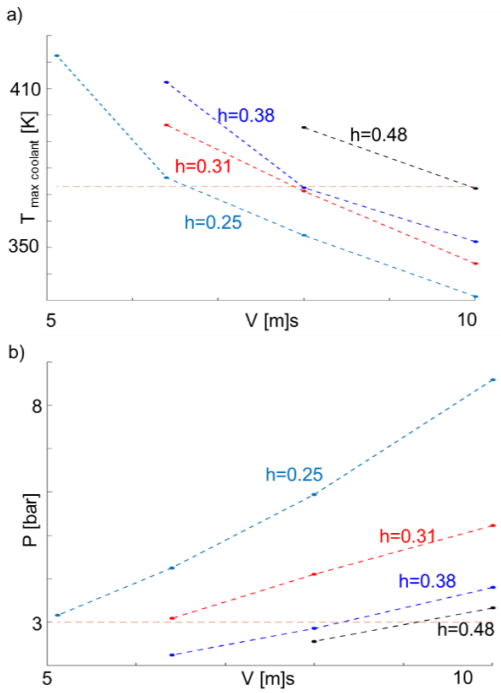


*Figure 7: a) Variation of maximum temperature in the outlet coolant channel. b) inlet total pressure required with varying inlet coolant velocity for different outlet channel height.*

Figure 7a shows the variation of maximum coolant temperature and inlet pressure requirement with changing inlet velocity for several outlet channel heights. For design constraints, the maximum temperature was set to 373K and 3 bar as maximum inlet pressure. These design points are marked by a horizontal line in Figure 7a and Figure7b respectively. Figure 7a shows a decrease in the maximum outlet channel coolant temperature as we decrease the channel height for the same inlet

velocity, and it can be seen a higher velocity, due to increased heat transfer coefficient, is more effective at reducing the maximum coolant temperature. Figure 7b plots the cost of this improved cooling in terms of the increased inlet pressure requirements which increases with increased inlet velocity and decreases as the channel height increases. Based on the results, a channel height of 0.38mm for the outlet channel was chosen with an inlet velocity of 8m/s as an optimal compromise between cooling and inlet pressure requirement.

With the parameters known for the outlet channel, the geometry at the bend channel, as depicted in Figure 8a was investigated. As evident from Figure 8b, even if the channel height is reduced at the bend, the coolant temperature does not drop to the desired value at 8m/s inlet velocity. At a higher velocity of 10m/s, the temperature drops to the desired temperature, but the cost in terms of increased pressure requirements increases it he channel height is decreased as evident in Figure 8c. From Figure 8c it is seen that even as the channel height is reduced and velocity is increased back to 10m/s, the maximum temperature is higher than the maximum design temperature. Figure 8d illustrates that the reason for these hot spots are the regions of low velocity leading to poor heat transfer.

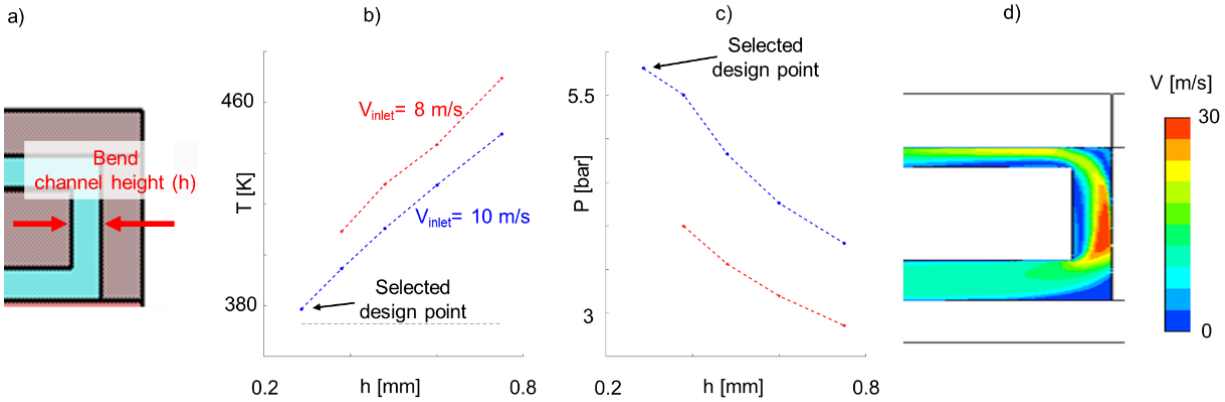


*Figure 8: a) Schematic showing the bend channel height. b) Variation of maximum coolant temperature. c) inlet total pressure required by changing the bend channel height for different inlet velocities. d) velocity contour in the bend channel highlighting the separation region and a low velocity leading to hotspot formation.*

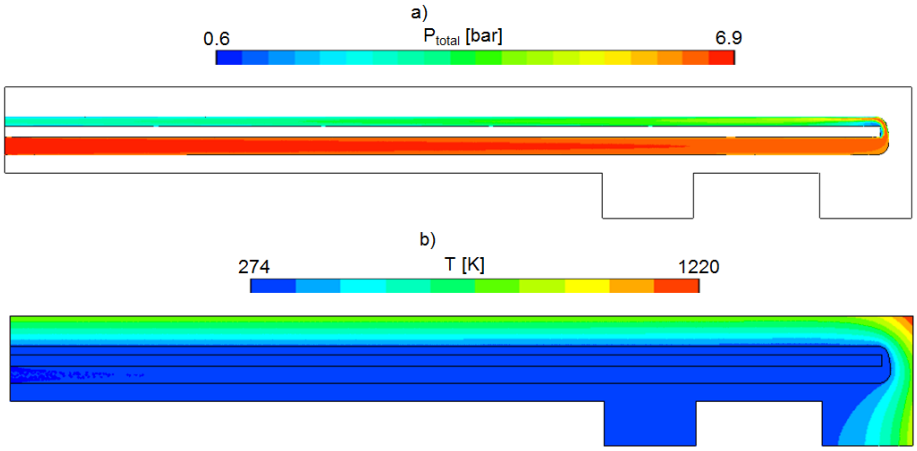


*Figure 9: a) Pressure contour of the coolant channel. b) Temperature contour of the system for the cooled geometry*

To prevent this separation of the coolant, the geometry at the bend was transformed into a circular arc at the bottom and a spline at the top which follows the velocity streamline. This bend decreased the maximum temperature by 7.7K compared to a 90 deg. bend, 2K below the maximum temperature threshold, with a smaller increase in pressure cost compared to only decreasing the channel height. Figure 9b shows the temperature contour of the complete probe and cooling assembly showing a maximum temperature on the outside of the system of 1220K. Figure 9a shows the pressure contour of the coolant showing the increased inlet total pressure requirement to 6.9bar. The temperature distribution of the coolant (Figure 10a) highlights that the highest temperature region lies in the upper bend of the channel. Figure 10b shows the velocity contour of a zoom in of the hottest region featuring a zone of low velocity and Figure 10c shows the corresponding temperature contour with a high temperature in the region of low velocity.

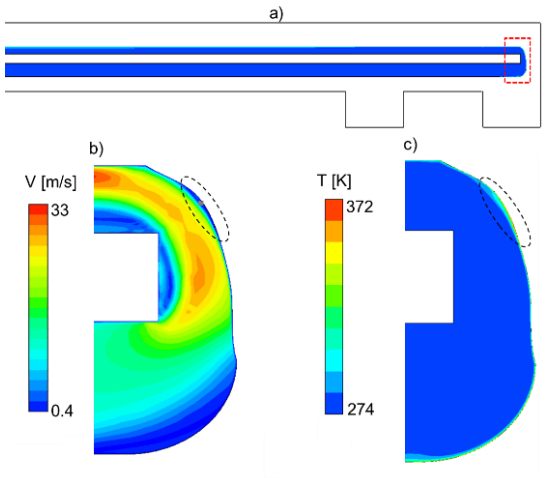


*Figure 10: a) Temperature contour of the coolant of the cooled geometry. b) Zoom on the velocity contour at the bend. c) Zoom on the temperature contour.*

## STRUCTURAL ANALYSIS - HOT TO COLD CONVERSION

A two-dimensional axisymmetric static stress analysis was carried out using Ansys static structural solver. The average values of the pressure and wall shear on each section of the channel wall was based on the conjugate heat transfer results of the previous section and applied as loads in the structural Finite Element Analysis (FEA) as depicted in Figure 11. The entire geometry was assigned to the temperature dependent properties of Inconel and the average temperature of each section of the cooling jacket and probe body, computed from the CFD analysis, was imposed in the FEA. The same axis of symmetry is applied and it is constrained from moving in the radial direction but free in the axial direction and the end of the probe is constrained from moving in the axial direction, though it is free to move in the radial direction as highlighted in Figure 11. Figure 12a and Figure 12b show the deformation in the axial and radial direction. The radial deformation is highest on the outer wall; however it is smaller in magnitude than the axial deformation. Figure 12c and 12d plot the contour of the normal and shear stress respectively. As expected most of the stress is concentrated at places where there are sharp changes in geometry, however the magnitude of these stress concentrations is below the yield strength of the material.

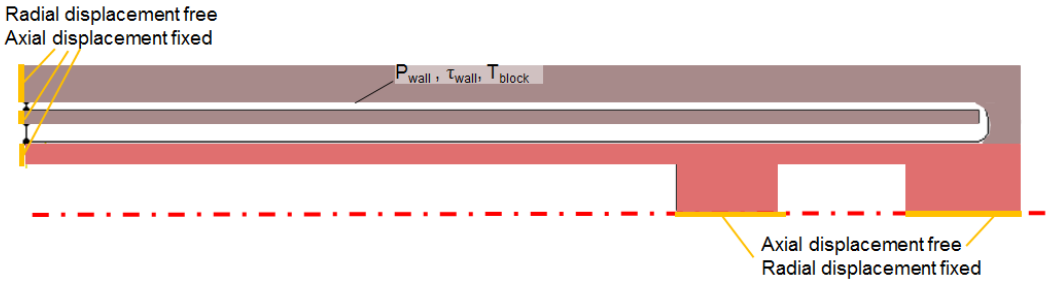


*Figure 11: Boundary Conditions for the 2D static structural analysis*

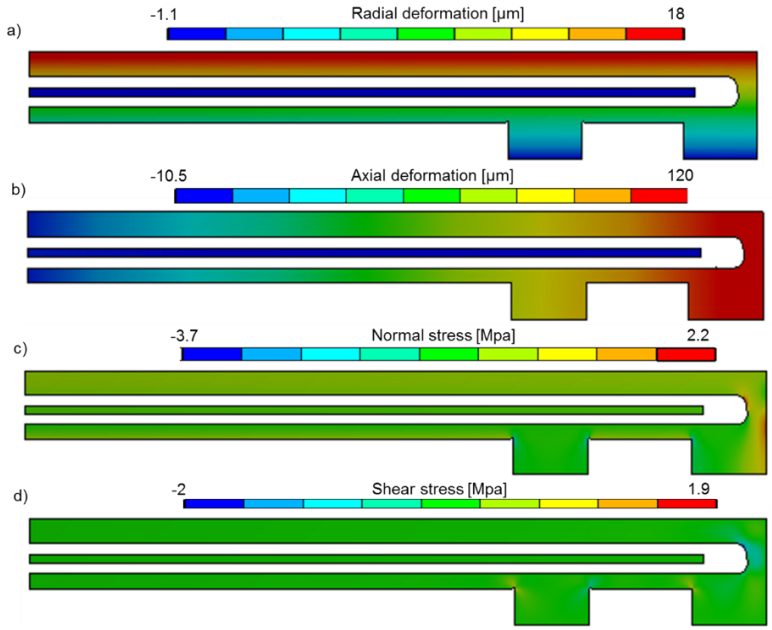


*Figure 12: a) Radial deformation of the first geometry. b) Axial deformation of the first geometry. c) Normal stress contour of the first cooled geometry. d) Shear stress contour of the first cooled geometry.*

To evaluate the effect of the deformation on the cooling performance, the deformation was applied to the baseline configuration and a conjugate heat transfer case was performed to evaluate the cooling performance of the deformed probe which yields in the coolant temperature contour for the deformed probe (Figure 13a). The most significant deformation is at the end of the probe where the flow turns. As observed in Figure 13b, the increase in dimensions generates a small flow separation, which leads to a hot spot generation in the flow, increasing the local temperature over the design maximum temperature as highlighted in Figure 13c

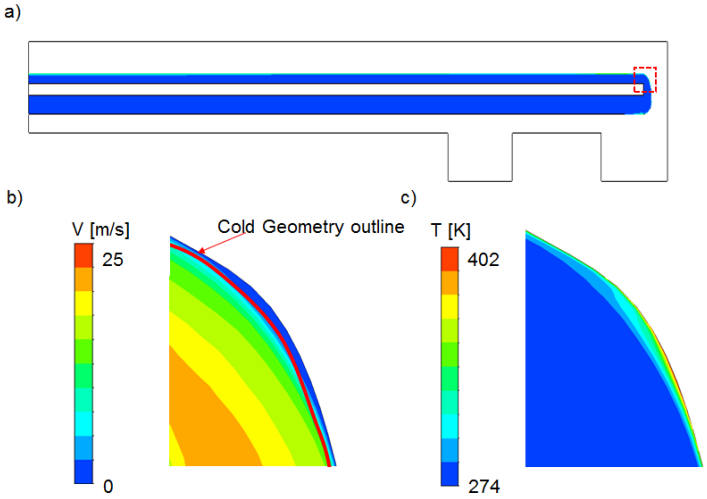


*Figure 13: a) Coolant temperature contour of the deformed geometry. b) Velocity contour of the zoom at the hottest part. c) Temperature contour of the zoom at hottest part*

Based on this information, the geometry of the bend was altered to take into account the deformation due to the coolant pressure and the differential heating of the probe. After several iterations of cold-to-hot conversions, outlined in Figure 14a, where the deformed or "hot" geometry is iteratively modified to obtain a new coolant flow field, an optimized geometry was retrieved that was able to cool the system in both cold and hot conditions. The temperature contour of the coolant in hot condition is depicted in Figure 14b with a zoom on of the hottest part (Figure 14c and Figure 14d) in which the temperature remains below the critical temperature.

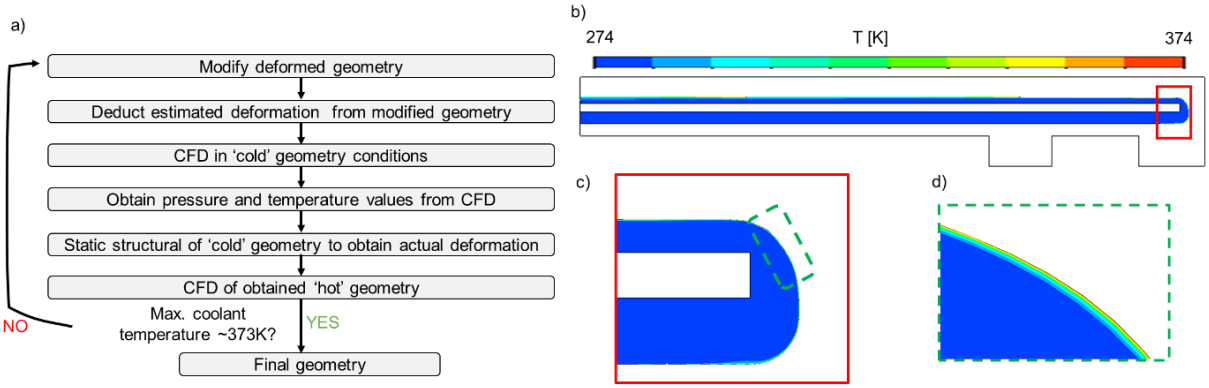


*Figure 14: a) Flow chart of the design process for the cold-to-hot conversion. b) Temperature contour of the deformed cooled geometry. c/d) zooms of the hottest part of the coolant channel*

## EXPERIMENTAL SETUP AT PETAL LAB

The experiments are carried out at the Purdue Experimental Turbine Aerothermal Laboratory, PETAL. The test facility contains two wind tunnels connected in parallel: an annular cascade, for turbine research, and a linear wind tunnel, for fundamental research and calibration of the instrumentation.

The lab offers the capability to go from low speed all the way to supersonic flow, hence offers the adequate range of Reynolds and Mach to perform probe calibration at conditions similar to turbine testing environment. The test section is located downstream of a settling chamber that is optimized to break the turbulent structures in the flow and generate a homogeneous flow. The lab is depicted in Figure 15.

The preliminary experiments were performed in the linear test section and has a rectangular cross section with dimension 170x230 mm. The walls that delimit the test section are made of quartz to have a fully optical accessible test section that

include the four corners. Further details about the design and the characteristics of the wind tunnels can be found in [19]. The conditions selected to test the probes are summarized in Table 1. The temperature of the flow and the mass flow are set upstream of the settling chamber by an air heater and an admission valve. The Mach number and the Reynolds number are obtained by relating the mass flow with the cross area of the downstream sonic valve in the calibrated linear test section [20].

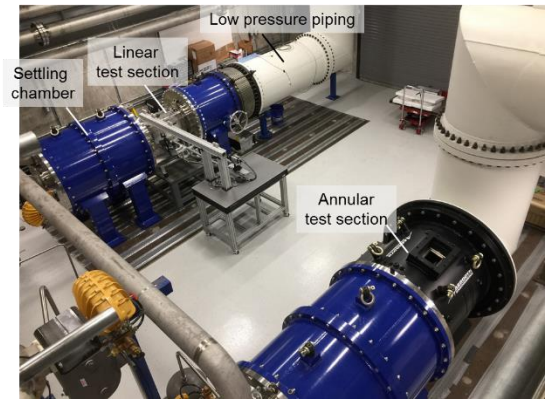


*Figure 15: View of the PETAL lab*

*Table 1: Summary of experimental conditions*

| Mass flow | Total Pressure | Total Temperature | Mach Number |
|---|---|---|---|
| 3.94 kg/s | 1.3 bar | 400 K | 0.25 |

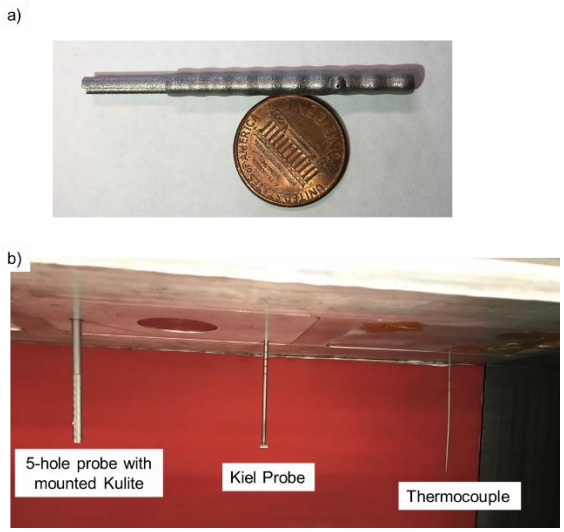


*Figure 15: a) Detail of the 3D printed probe. b) The test section with the instrumentation*

The probe frame is 3D printed in Inconel 718 due to the difficulty to machine the internal channels. In the assessed experiments we inserted one Kulite in the base pressure orifice (Kulite 4 in Figure 2).

Figure 16 depicts the probe inserted in the wind tunnel through the top wall, and located in the center of the test section to minimized the wall effects. The total temperature of the flow was measured with a total pressure Kiel probe and the total temperature with a thermocouple probe located downstream of the high frequency 5 hole probe. First, the Kulites were calibrated by using several vacuum levels and afterwards they were inserted in the five-hole probe. In the first tests, we focused on the analysis of the low frequency reading of the Kulite sensor for the two 5-hole probes Figure 17a depicts the calibration of the Kulite for several vacuum conditions ($R^2$ value: 0.99997). Figure 17 plots the low frequency signal of the Kulite in function of time. Total test time was around 30 seconds per condition.

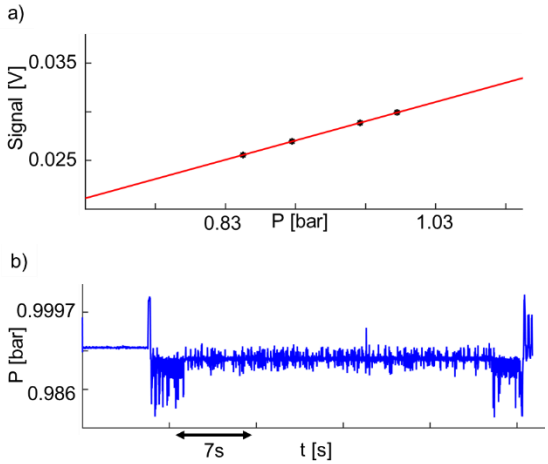


*Figure 16: a) Calibration of the Kulite. b) Low frequency signal of the Kulite sensor*

Once the proper operation of the Kulite has been ensured, the next steps will be to analyze the high frequency data, comparing the frequency content of the novel wavy five hole probe with the traditional cylindrical probe. The calibration map of the probe will be extracted and used as input in a software package that can provide the velocity direction, Mach number and pressure in real time.

## CONCLUSIONS

In this paper a novel design approach for cooled miniature fast five hole probe is discussed. In a first step, the probe dimensions were selected to minimize the interference with the flow field. Afterwards, a numerical approach was outlined to be able to cool the probe for high temperature conditions. This included a two dimensional parametric study in which the geometrical as well as inlet conditions were analyzed. Structural issues were addressed and a cold-to-hot conversation strategy was outlined. Finally, calibration and first tests in the Purdue Experimental Turbine Aerothermal Lab was discussed.

## ACKNOWLEDGEMENTS

The authors want to thank Nyansafo Aye-Addo for his help to set up the Kulite system.

## REFERENCES

[1] Ainsworth, R. W.; Miller, R. J.; Moss, R. W. and Thorpe, S. J.; 2000. "Unsteady Pressure Measurement". Measurement Science and Technology, 11(7), pp. 1055-1076. DOI: 10.1088/0957-0233/11/7/319

[2] Sieverding, C.H.; Arts, T.; Denos, R., and Brouckaert, J. F.; 2000. "Measurement Techniques for Unsteady Flows in Turbomachines," Experiments in Fluids, 28(4), pp. 285-321. DOI: 10.1007/s003480050390

[3] Bryer, D.W. and Pankhurst, R. C.; 1971. "Pressure Probe Methods for Determining Wind Speed and Flow Direction". Her Majesty's Stationary Office, Norwich, UK.

[4] Arguelles Diaz, K.M.; Fernandez Oro, J. M.; Blanco Marigorta, E. and Barrio Perotti, R.; 2010. "Head geometry effects on Pneumatic three-hole pressure probes for wide angular range," Flow Measurement and Instrumentation, 21, pp. 330-339. DOI: 10.1116/j.flowmeasinst.2010.04.004

[5] Delhaye, D.; Paniagua, G.; Fernandez Oro, J. M. and Denos, R.; 2011. "Enhanced Performance of Fast-Response 3-Hole Wedge Probes for Transonic Flows in Axial Turbomachinery," Experiments in Fluids, 50(1), pp. 163-177. DOI: 10.1007/s00348-010-0908-y

[6] Liu, Z., and Paniagua, G., 2018, "Design of Directional Probes for High-Frequency Turbine Measurements," Journal of Engineering for Gas Turbines and Power, 140(1), p. 011601. DOI:10.1115/1.4037640

[7] Paniagua, G. and Denos, R.; 2002. "Digital Compensation of Pressure Sensors in the Time Domain," Experiments in Fluids, 32(4), pp. 417–424. DOI: 10.1007/s003480100355

[8] Bergh, H. and Tijdeman, H.; 1965. "Theoretical and Experimental Results for the Dynamic Response of Pressure Measuring Systems," National Aero- and Astronautical Research Institute, Amsterdam, The Netherlands, NLR-TR F.238. DOI: 10.13140/2.1.4790.1123

[9] Hanke, W.; Witte, M.; Miersch, L.; Brede, M.; Oeffner, J.; Michael, M.; Hanke, F.; Leder, A. and Dehnhardt, G.; 2010. "Harbor seal vibrissa morphology suppresses vortex-induced vibrations," The Journal of Experimental Biology, 213, pp. 2665-2672. DOI: 10.1242/jeb.043216

[10] Hans, H.; Miao, J. M.; Triantafyllou, M. and Weymouth, G.; 2013. "Whisker-like Geometries and Their Force Reduction Properties," MTS/IEEE-OCEANS, June 10-14, Bergen, Norway. DOI: 10.1109/OCEANS-Bergen.2013.6608113

[11] Kottapalli, A. G. P.; Asadnia, M.; Miao, J. M. and Triantafyllou, M. S.; 2015. "Harbor Seal Whisker Inspired Flow Sensors to Reduce Vortex-Induced Vibrations," 28th IEEE International Conference on Micro Electro Mechanical Systems, January 18-22, Estoril, Portugal. DOI: 10.1109/MEMSYS.2015.7051102

[12] Alvarado, P. V.; Subramaniam, V. and Triantafyllou, M.; 2013. "Performance Analysis and Characterization of Bio-Inspired Whisker Sensors for Underwater Applications," IEEE/RSJ International Conference on Intelligent Robots and Systems, November 3-7, Tokyo, Japan. DOI: 10.1119/IROS.2013.6697220

[13] Beem, H.; Hildner, M. and Triantafyllou, M.; 2013. "Calibration and validation of a harbor seal whisker-inspired flow sensor," Smart Materials and Structures, 22, p. 014012. DOI: 10.1088/0964-1726/22/1/014012

[14] Beem, H. R.; Triantafyllou, M. S.; 2015. "Wake-induced 'slaloming' response explains exquisite sensitivity of seal whisker-like sensors," Journal of Fluid Mechanics, 783, pp. 306-322. DOI: 10.1017/jfm.2015.513

[15] Pai, Y.; Prasad, A.; Fernandes, R. and Ricklick, M.; 2017. "Preliminary Investigation of Bio-Inspired Cylinders for Improved Thermal Performance of Internal Cooling Channels," 53rd AIAA/SAE/ASEE Joint Propulsion Conference, July 10-12, Atlanta, GA. AIAA 2017-4977. DOI: 10.2514/6.2017-4977

[16] Richter, A. and Naudascher, E.; 1976. "Fluctuating Forces on a Rigid Circular Cylinder in Confined Flow," Journal of Fluid Mechanics, 78(3), pp. 561-576. DOI: 10.1017/S0022112076002607Churchill, S., and Bernstein, M., 1977, "A Correlating Equation for Forced Convection From Gases and Liquids to a Circular Cylinder in Crossflow," Journal of Heat Transfer, 99(2), pp.300-306. DOI. 10.1115/1.3450685

[17] Bejan, A.; 2013: "Convection Heat Transfer". 4th edition, John Wiley & Sons

[18] Paniagua G.; Cuadrado, D. G.; Saavedra, J.; Andreoli, A.; Meyer, A.; Solano, J. P.; Herrero, R.; Meyer, S. E. and Lawrence, D.; 2018. "Design of the Purdue Experimental Turbine Aerothermal Laboratory for Optical and Surface Aero-Thermal Measurements," Journal of Engineering for Gas Turbines and Power, Accepted Manuscript, DOI: 10.1115/1.4040683

[19] Cuadrado D. G.; Saavedra J.; Andreoli V. and Paniagua G.; 2017. "Experimental Calibration of a High Speed Blowdown Tunnel," ISABE-2017-22636